Project 9: Delamerian orogen mineral potential mapping Cu-Mo-Au mineral system

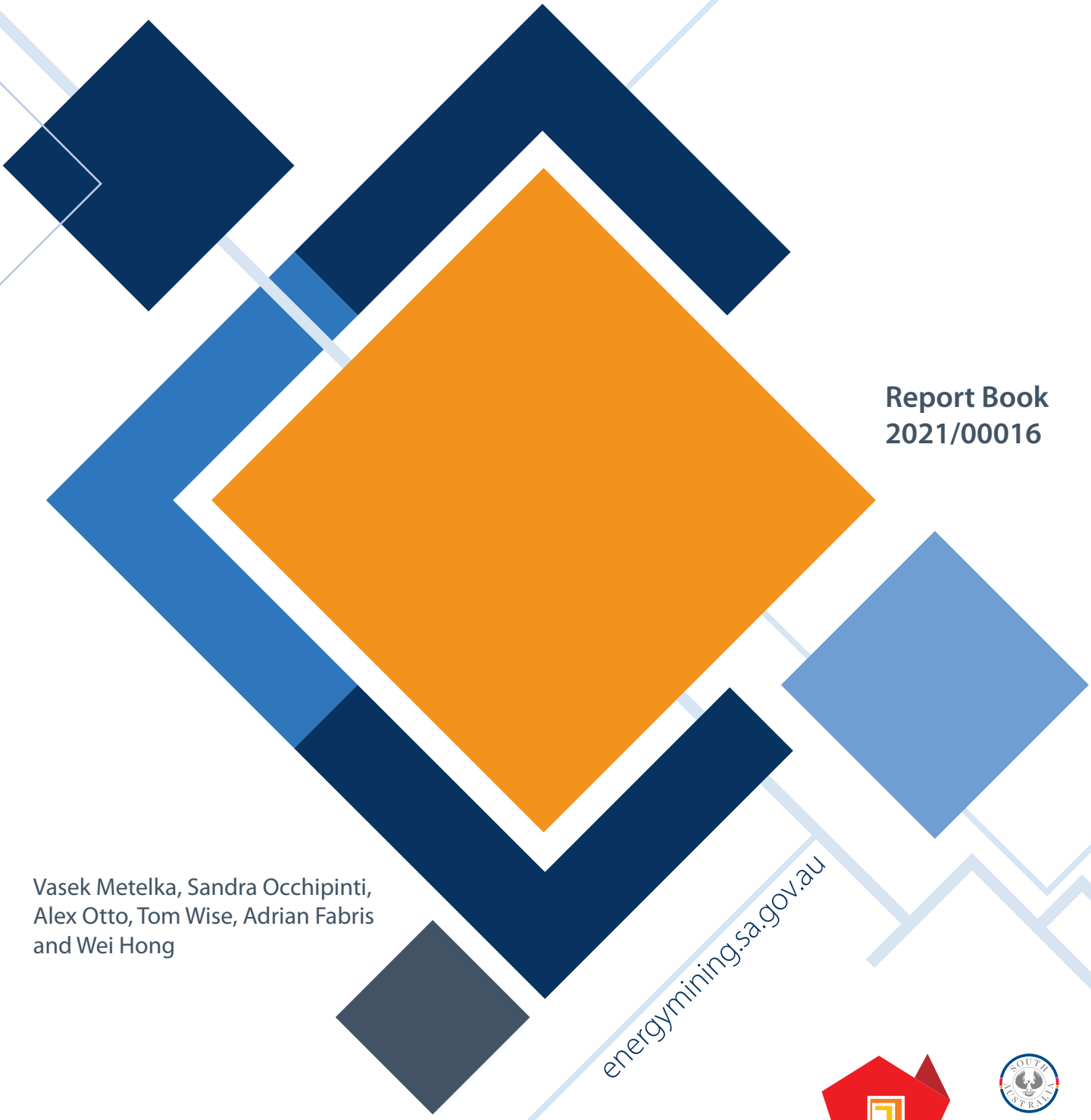

Report Book 2021/00016

Vasek Metelka, Sandra Occhipinti, Alex Otto, Tom Wise, Adrian Fabris and Wei Hong

energymining.sa.gov.au

MinEx CRC

SOUTH AUSTRALIA

Government of South Australia
Department for Energy and Mining

MinEx CRC Limited
26 Dick Perry Avenue, Kensington, WA, 6151
PO Box 1130, Bentley, WA, 6102, Australia
admin@minexcrc.com.au

ABN: 66 625 533 913

Interim Technical Report

Project 9: Delamerian orogen mineral potential mapping

Cu-Mo-Au mineral system

Authors:

Vasek Metelka, Sandra Occhipinti, Alex Otto
MinEx CRC, CSIRO Mineral Resources

Tom Wise, Adrian Fabris
MinEx CRC, GSSA

Wei Hong
MinEx CRC, Adelaide University

November 2021

MinEx CRC Report 2021/63
Department for Energy and Mining Report Book 2021/00016

Australian Government
Department of Industry, Innovation and Science

Business Cooperative Research Centres Program

EXECUTIVE SUMMARY

A mineral systems analysis for Cu-Mo-Au in the Delamerian Orogen was conducted to assess its mineral potential. A conceptual model was delineated, and prospectivity maps were created. These maps can serve partially for drill and sampling campaign targeting. The conceptual model is implemented as a flexible workflow in ArcGIS, and it can be readily updated with new data.
Several critical elements of the conceptual model will be reassessed when more detailed geochemical, mineralogical, petrophysical, and structural data will be available after the MinEx NDI drilling campaign. The fractionation and oxidation state of the mapped intrusive/volcanic bodies will be better estimated by direct measurement and new sampling of the geochemical properties of rocks from the drill chips and drill core or surface mapping. Similarly, numerical simulation and 3D geological modelling will confirm or disprove the proposed model, which supports structures that traverse most of the lithospheric crust
Of primary interest for the upcoming sampling campaign should be the extent and nature of the interpreted Mount Wright Volcanics and other contemporaneous intrusive and volcanic suites related to the Delamerian arc or back-arc development. The studies can be further focused on zones that are traversed by the interpreted crustal-scale discontinuities.

OBJECTIVE(S)	RESULT(S)
Conduct mineral systems analysis and mapping for the Delamerian Orogen NDI study areas.	Cu-Mo-Au mineral system prospectivity maps and model
NEXT STEP(S)	**TIMING**
Conduct same for Ni-Cu-PGE and Cu-Pb-Zn mineral systems, update existing model based on new data	List timing against next steps

MINEX CRC MILESTONES
CY20Q3; RP3.3.32
UTILISATION/COMMERCIALISATION OPPORTUNITIES
Guiding NDI drilling Gap analysis for new data acquisition
IP
N/A
CONFIDENTIALITY
N/A
APPROVED BY
Name of person who approved the report and date of approval. Interim Technical Reports and Final Project Reports can be approved by Project Leader, Program Leader or CEO.

Table of Contents

Table of Contents 3

1 Introduction 4

2 Geological Background 4

2.1 The geology of the Delamerian Orogen 4
2.2 Cu-Mo-Au Mineral system 5
3 Methodology 8

3.1 Derivation of the spatial evidence layers 9
3.2 The fuzzy inference network 15
4 Results & Discussion 17

5 Conclusions 19

6 Acknowledgements 20

7 References 20

1 Introduction

The Delamerian Orogen traverses a considerable section of the Australian continent from Tasmania to the Australian mainland (Raymond et al., 2018). MinEx CRC and the associated National Drilling Initiative (NDI) selected a part of the Delamerian Orogen in South Australia as one of the target areas (Fig 1.) where newly developed techniques and technology should be tested to advance our understanding of the geotectonic evolution of the orogen as well as its mineral potential.
In eastern South Australia, beneath the Murray Basin, the Delamerian Orogen is considered prospective for porphyry-style Cu-Mo-Au deposits associated with subduction and post-subduction related magmatism (e.g., Bookstrom et al., 2014). A recently completed interpreted geological basement map (Wise, 2020) provides a framework to evaluate the potential for this deposit style, with the particular aim of assessing prospectivity beneath sedimentary cover before planned NDI drilling[1].
This report is a short technical summary of a desk study undertaken to evaluate and spatially map the potential of favourable conditions for processes interconnected with the formation of Cu-Mo-Au mineral systems found in and around primarily subduction-related magmatic and volcanic centres. Other mechanisms related to the formation of fertile magmas by remelting subduction metasomatised subcontinental lithospheric mantle such as post-collisional crust thickening, mantle delamination or lithospheric extension (Richards, 2009; John et al., 2010) can also be considered. Since the number of currently found deposits, mines, and promising occurrences was considered too low compared to districts amenable to conducting a data-driven assessment, a knowledge-based approach was selected to create a first pass mineral potential map.

[1]https://www.energymining.sa.gov.au/minerals/geoscience/geological_survey/gssa_projects/delamerian_ndi

2 Geological background

2.1 The geology of the Delamerian Orogen

The Delamerian Orogen (514–490 Ma) marks the deformed continental margin of the supercontinent Gondwana. Located to the east of the Neoproterozoic Adelaide Rift Complex (Fig 1.), Neoproterozoic-Cambrian passive margin and rift sequences were subjected to magmatism metamorphism and deformation associated with the Delamerian Orogeny during the transition to an active subduction margin (Rosenbaum, 2018).
The Delamerian Orogen is generally poorly exposed and is covered by up to 600 m of Murray Basin fluviolacustrine–aeolian to marine sediments (Brown and Stephenson, 1989; Geoscience Australia, 2017), as well as by isolated Mesozoic-Palaeozoic depocentres (Alley, 1995; Rogers, 1995).
In the southern Mount Lofty Ranges, Neoproterozoic and Cambrian successions of the Adelaide Rift Complex and Normanville and Kanmantoo groups in the Kanmantoo Trough were metamorphosed to amphibolite facies and exhumed in a west-verging fold and thrust belt (Alias et al., 2002; Offler and Fleming, 1968; Sandiford et al., 1990; Flöttmann et al., 1994). Bimodal magmatism accompanied deformation (Foden et al., 2002), but also pre- and post-dates the Delamerian Orogeny across the broader orogen (Foden et al., 2020).
Limited data from sparse drilling through Murray Basin cover has resulted in poor spatial data distribution of the Delamerian Orogen. This is particularly true in the case of eastern South Australia, where much of the understanding of the orogen has been interpreted using geophysical interpretation between outcropping regions in the Mount Lofty Ranges, the Koonenberry Belt in western New South Wales, and the Stavely Zone in Victoria (as well as by analogy from Tasmanian equivalents).

Common geophysical expressions of the remnants of volcanic arcs active during the Delamerian Orogeny (the c. 510 Ma Mount Wright Volcanics in the Koonenberry Belt; Greenfield et al., 2011; Johnson, Phillips and Allen, 2016 and the c. 520–500 Ma Mount Stavely Volcanic Complex in Victoria; Cayley et al., 2018) extend into the South Australian portion of the Delamerian Orogen that is beneath younger sedimentary cover (e.g., Wise, 2020).

2.2 Cu-Mo-Au mineral system

The mineral systems approach, first established by Wyborn et al. (1994), evolved through several variations but essentially remains very similar, capturing and describing main processes and critical elements that 1) supply metals and ligands into the system (common fertility elements) 2) provide energy to drive fluid or melt flow (geodynamic throttle), 3) control and focus the fluid or melt flow (lithospheric architecture), 4) control the precipitation or crystallisation of economic minerals (depositional site), and 5) affect the preservation of the mineralised zones (preservation). Occhipinti et al. (2016, 2020) use conceptualised this into the mineral systems diamond (Fig. 2), but other concepts can be used as in McCuaig et al. (2010) or Skirrow et al. (2019). Using the above approach, critical processes and elements of these processes were derived for the Cu-Mo-Au model.

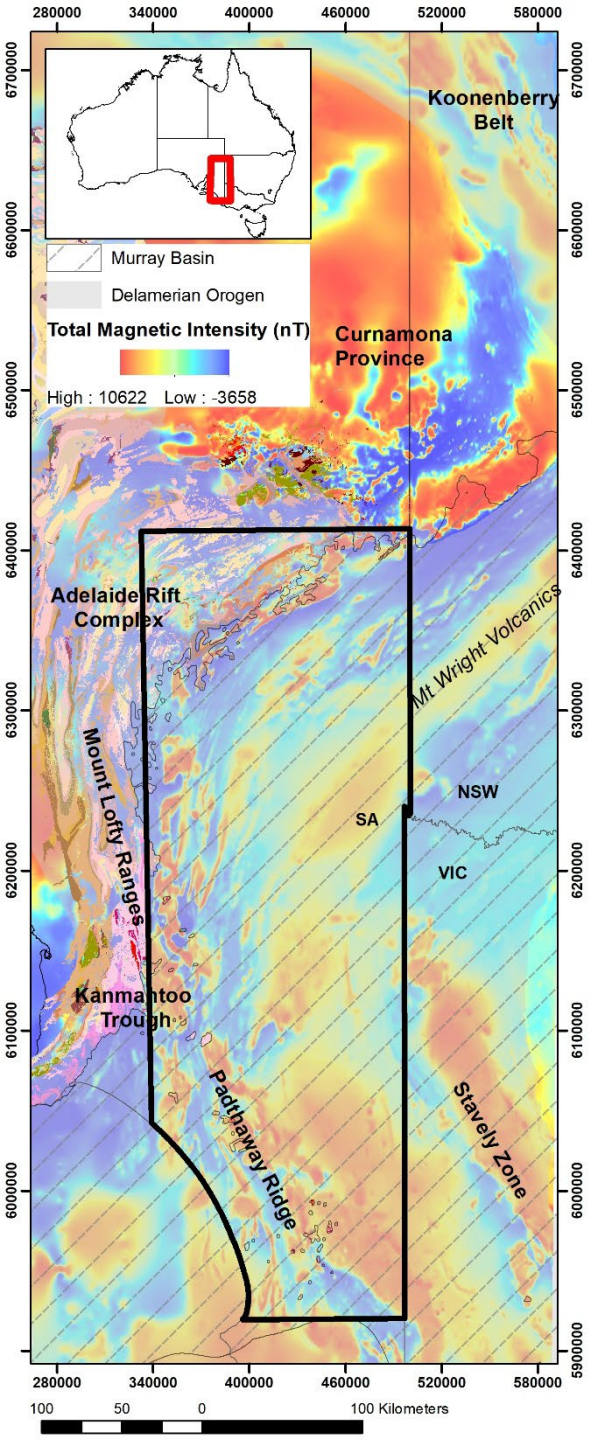

Figure 1 *1 Location map of the Delamerian Orogen (grey shaded region) showing the study area (solid black polygon) largely under cover of the Murray Basin. Solid-fill polygons represent outcropping basement geology.*

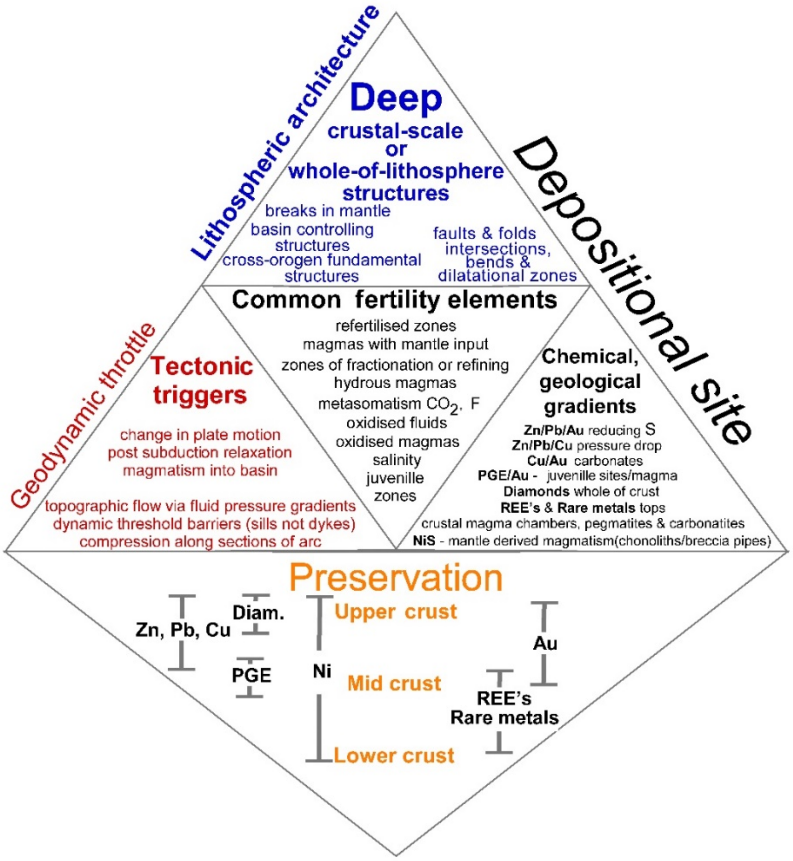

Figure 2 The mineral systems diamond, highlighting the generic constituent processes and critical elements of mineral systems from Occhipinti et al. (2020).

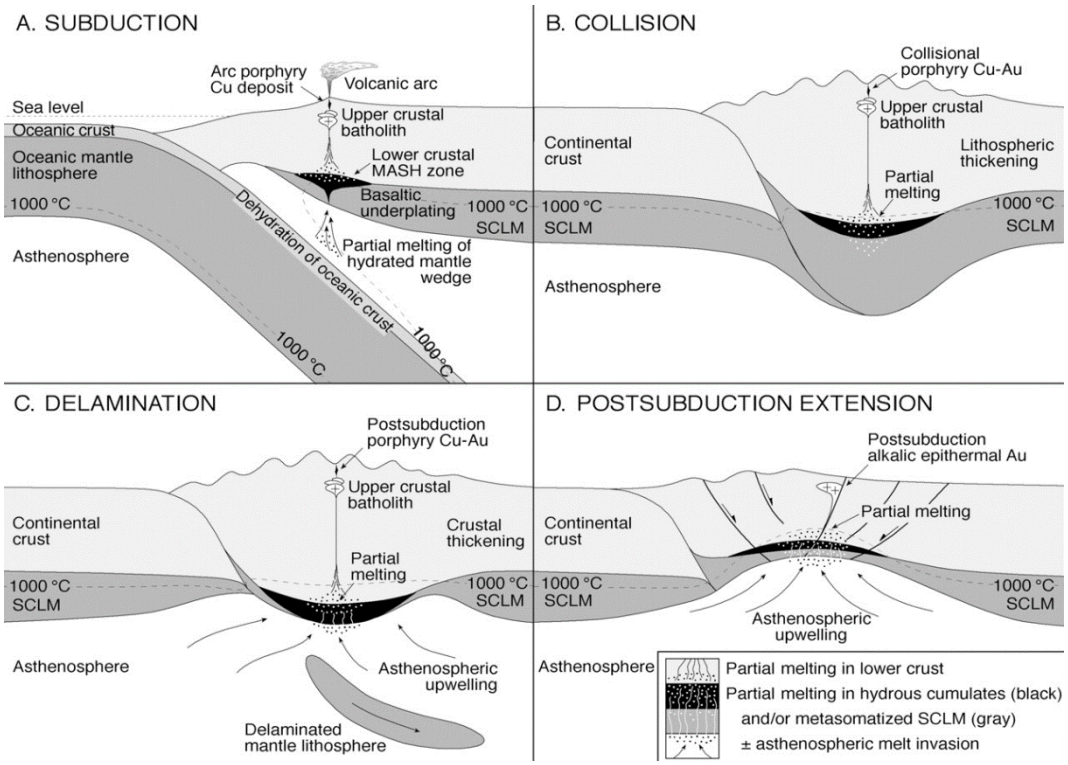

Figure 3 Plate tectonic setting of porphyry copper deposits from Richards (2009).

The Cu-Mo-Au mineral system model, established for the Delamerian NDI, primarily builds on the observations and descriptions for the porphyry copper system model (Figs. 2 and 3) of Sillitoe (2010) and findings, descriptions, and references presented and cited in the works of Richards (2009), John et al. (2010), Wilkinson (2013), or Lee and Tang (2020).

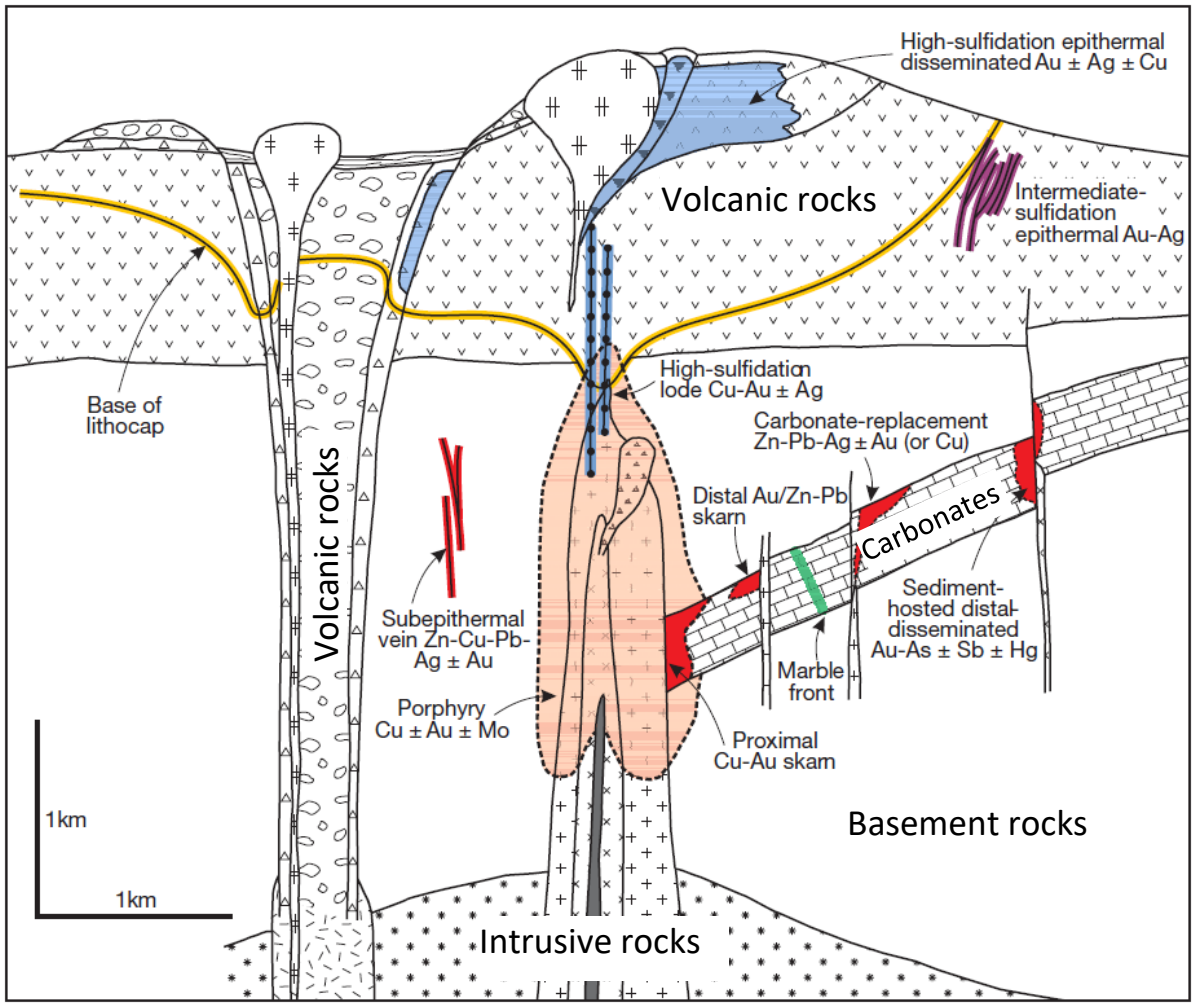

Figure 4 The porphyry Cu system model, depicting spatial relationships between different styles of mineralisation modified from Sillitoe (2010).

The common fertility elements mainly aim at processes that affect the availability and solubility of Cu and S in the system. In general, these processes can involve partial melting of an enriched lower crust that produces hydrous, S- and Cl-rich fluids and melts, ponding of the hydrous melts in the upper crust to form batholiths and plutons and subsequent exsolution of enriched magmatic and hydrothermal fluids that can carry metals (Fig. 3).

The geodynamic throttle is closely tied to the fertility elements because the arc magmatism is the primary energy driver; however, post-subduction lower crustal melting (Fig. 3) is caused by further compression or SLCM (SubContinental Lithosperic Mantle) delamination and subsequent extension could potentially also be considered.

The overall lithospheric architecture seems to play an important role as well. According to John et al. (2010), regional-scale fault zones show association with the location of porphyry copper deposits. Of particular interest are the oblique structures and intersection of these with the main thrusts. Piquer et al. (2021) confirm the alignment of PCD related plutons along major structural corridors and highlights the importance of misoriented oblique faults.

Because most primary PCD mineralisation remains very close (within first kilometres, see Fig. 4) to the source intrusive/volcanic centre (Sillitoe, 2010), essentially, most surface or near-surface fertility

components can also be considered favourable depositional environments. Reactive rocks such as carbonates that could host the associated mineral deposit styles, e.g., skarn, replacement type (Sillitoe, 2010), were also considered. Similarly, favourable host structures that can localise epithermal fluids associated with more distal parts of the porphyry copper mineral system were extracted and used.

3 Methodology

The methodology used closely follows that of Occhipinti et al. (2016) and Occhipinti et al. (2020) as well as Skirrow et al. (2019). In the first step, spatial evidential layers were derived from the available geological and geophysical data representing the evidence of critical processes occurring in a particular area. This was followed by combining the evidential layers in a fuzzy inference network to produce an overall mineral potential map. All layers were weighted according to applicability and confidence. The applicability weight refers to a criterion that describes how well a particular spatial evidence layer corresponds to its theoretical counterpart in the conceptual mineral system model. Creating spatial evidence layers usually involves imperfect proxies due to the inherent uncertainty and ambiguousness associated with the usually modelled/interpolated, or interpreted data. The confidence weight addresses this imperfect relationship by assigning combined confidence in the primary data, their accuracy, or the confidence in the process of derivation of the evidence layer. An overall importance weight is used for the overarching mineral system component. For the Cu-Mo-Au mineralisation, the fertility and geodynamic driver processes were considered most important, while crustal architecture and depositional site processes were deemed less important, particularly for large mineral systems. This is consistent with the PCD system models (e.g., Sillitoe, 2010; Richards, 2009; Wilkinson, 2013, or Lee and Tang, 2020), where the intrusive magmatic processes and the transient geodynamic triggers related to the subducting plate play the most critical role. The significance of structural control (John et al., 2010; Piquet 2021) and depositional site (Sillitioe, 2010) processes is less well established and particularly depositional gradients are more applicable to the smaller associated mineralisation styles. The weighting system utilised the Sherman-Kent scale (Jones and Hillis, 2003) for comparative weighting of factors that transform qualitatively perceived probability into numerical values ranging between zero and one (Tab. 1).

Table 1 Sherman-Kent Scale for quantifying importance, applicability and confidence weights modified from Jones and Hillis (2003).

Quantitative probability range	**Mean probability(weight)**	**Perceived qualitative probability**
0.98-1	0.99	proven; definitely true
0.9-0.98	0.94	virtually certain; convinced
0.75-0.9	0.83	highly probable; strongly believe; highly likely
0.6-0.75	0.68	likely; probably true; about twice as likely to be true as untrue; chances are good
0.4-0.6	0.50	chances are about even, or slightly better than even or slightly less than even
0.2-0.4	0.30	could be true but more probably not; unlikely; chances are fairly poor; two or three times more likely to be untrue than true
0.02-0.2	0.11	possible but very doubtful; only a slight chance; very unlikely; very improbable
0-0.02	0.01	proven untrue; impossible

3.1 Derivation of the spatial evidence layers

The spatial model of the mineral system was constructed to have the same extent as the newly interpreted geological map (Wise, 2020). The model cell size is 100 m resulting in rectangular dimensions of 5007 rows and 1871 columns. The cell size was selected as an optimal balance between the resolution of the primary interpretative data and the regional scale of the prospectivity study. The critical elements for fertility (Tab. 2) were primarily derived from the geological reinterpretation of the area (Fig. 5; Wise, 2020), mainly drawing on airborne magnetic data (Katona, 2020) and their derivatives (shaded relief, directional derivatives, reduction to the pole). Intrusive and volcanic units that could be associated with volcanic centres were selected and weighted according to their affinity to subduction or post-subduction related magmatism. The Anabama and Bendigo granitoid intrusions showing Au-Cu mineralisation were rated highest (Fig. 5a).

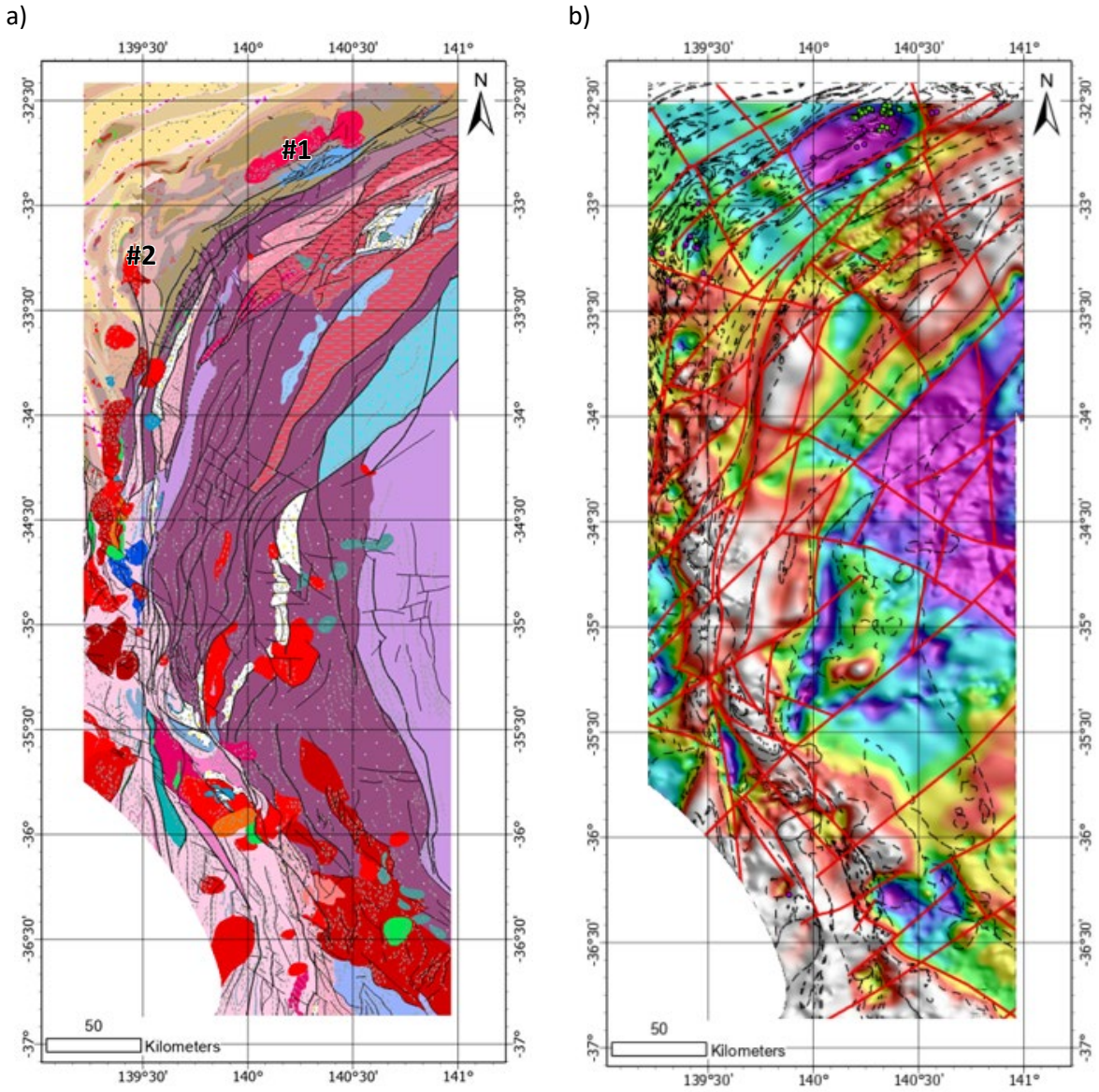

Figure 5 a) New lithostratigraphic interpretation derived based on integrated interpretation of magnetic and gravity data (after Wise, 2020) for detailed legend refer to Wise (2020), #1- Anabama intrusion, #2 Bendigo intrusion; b) major crustal-scale structures (in red) overlain on the shaded Bouguer anomaly map (Katona, 2020; dashed lines represent lithological boundaries from a).

Contemporaneous, predominantly intrusive, and volcanic rocks followed, and other volcanic rocks or mixed type units were assigned lower weights. The Euclidean distance to the outline of the units was calculated for every set of lithostratigraphic units. The distance raster was then reclassified into three classes representing the presence of the critical component, a 5 km buffer of influence of intermediate probability, and the areas beyond the 5 km buffer zone. The five km buffer zone was selected as the approximate maximum distance of fluid migration from the parent volcano-intrusive centre (Sillitoe, 2010).

The AusLAMP magneto-telluric inversion data (Robertson et al., 2020) that characterise the resistivity of the lithosphere and mantle in the area were analysed, and low resistivity domains were mapped. Two components were considered: 1) close to the lower crust/upper mantle boundary (Fig. 6a) and 2) in the middle crust (Fig. 6b).

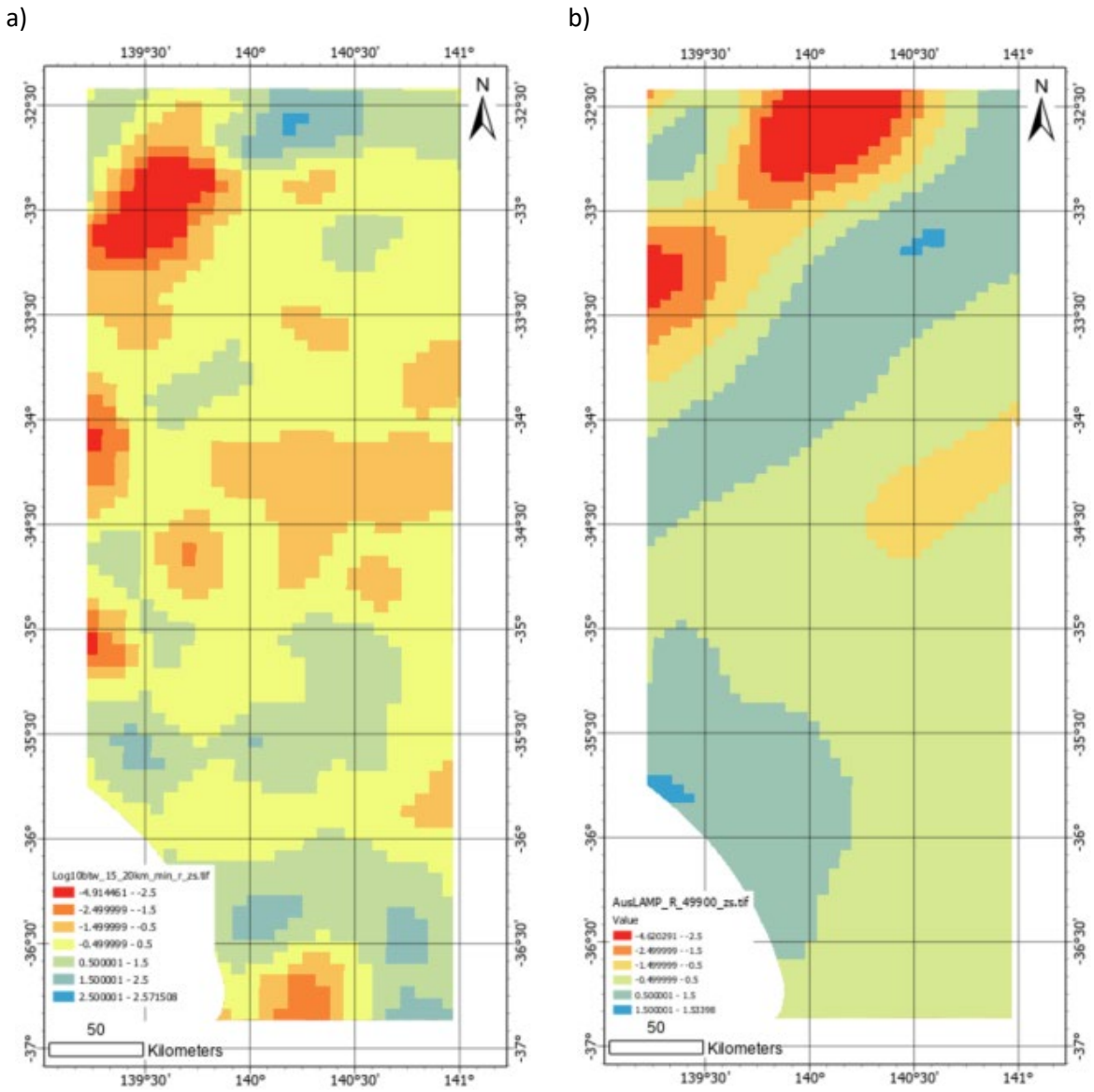

Figure 6 a) Possible middle crust magma ponding regions approximated by low resistivities (red colour) of the AusLAMP model (after Robertson et al., 2020) between 15-20 km; b) Source regions of hydrous magma at SLCM boundary approximated by low resistivities (red colour) in the AusLAMP model 49900m depth slice.

Both of these could represent relict hydrous intrusive bodies related to fertile magma differentiation and magma ponding. The mapping of hydrous (hydrogen-rich) material through MT resistivity was proposed in the work of, e.g., Selway (2014). For the lower crust upper mantle boundary, the 49900 m depth slice was used, while the minimum aggregated resistivity for the depth slices between 15 and 20 km was derived from the 3D model cube. The lower crustal layer was standardised (Z-score transformed) and divided into six classes based on the standard deviation from the mean; the lowest resistivity class was considered most prospective. The 15 to 20 km aggregated data showed a highly right-skewed distribution and hence was first log-transformed and then standardised. Seven classes were derived based on the standard deviation from the mean (+-0.5 SD, +-1.5 SD, +-2.5 SD), with the lowest resistivity class again representing most prospective regions. This transformation and classification were utilised to highlight anomalous regions in the data.

The crustal architecture critical elements (Tab. 2) were extracted as deep, crustal-scale structures that could have impacted the emplacement of magmatic intrusions and the localisation of the volcano-intrusive centres. These structures were interpreted from the available Bouguer Anomaly map and its derivates (shaded relief, vertical derivative) (Katona, 2020). The structures were separated based on their orientation to the overall orientation of the orogen's structural grain, which potentially corresponds to the original geometry of the subduction zone. Orogen oblique and orogen parallel structures were treated separately. Additionally, intersections of all the crustal-scale structures were computed. Euclidean distance rasters were computed to the three components, and each was reclassified into six classes based on distance with a step of 1.5 km extending up to 7.5 km away from each structure, creating a buffer of influence of 15km. The buffer distance was selected to reflect the influence zone of the physical processes as well as the uncertainty in the location of the actual fault trace and dip direction of these structures. The innermost class was assigned the highest prospectivity and the outermost class the lowest. The applicability weights of the orogen oblique structures and the intersection of structures were higher than the orogen parallel structures.

MinEx CRC Limited
26 Dick Perry Avenue, Kensington, WA, 6151
PO Box 1130, Bentley, WA, 6102, Australia
admin@minexcrc.com.au

ABN: 66 625 533 913

Table 2 Mineral systems analysis overview table with processes, components and derived spatial evidence layers and their attributed weighting parameters.

Mineral system component	Process	Critical component theoretical	Critical component mappable	Derivation of mappable critical components	Classes within the evidential layer	Importance weight	Applicability weight	Confidence weight	Overall weight
Common fertility elements/Geodynamic throttle	Partial melting of hydrated mantle or partial melting of enriched lower crust to produce hydrous, S-rich fluids and melt; Ponding of hydrous melt in the upper crust forming plutons or batholiths; exsolution of magma to produce magmatic-hydrothermal brines and vapour phases that carry metals, fluids, and ligands. Magmatism/volcanism drives fluid flow during subduction, post-subduction compression or SCLM delamination and post-subduction extension.	mostly calc-alkaline or high-K calc-alkaline to alkaline intrusives and volcanics; hydrous oxidised nature, I-type magnetite series / arc-related magmatism and volcanism or post-subduction melting driving magma ascent through crust and fluid flow	intermediate to felsic intrusives related to subduction and post-subduction extension with clear evidence of mineralisation processes occurring	distance to EOda Anabama and Bendigo Granites	three classes established based on empirical class breaks (>5 km = low(1), 5-0.001 = medium(2), <0.001 km = high(3))	0.99	0.94	0.83	0.772
			intermediate to felsic volcanics and intrusives related to subduction or post-subduction extension, showing oxidised nature	distance to Egnv - Mount Wright Volc., EOd25 – undiff. granitic-granodioritic intrusions	three classes established based on empirical class breaks (>5 km = low(1), 5-0.001 = medium(2), <0.001 km = high(3))	0.99	0.83	0.68	0.559
			intermediate to felsic volcanics and intrusives possibly related to subduction or post-subduction extension, mostly showing oxidised nature	distance to Epov - Bittles Tank Volc., EOd1 - undiff. felsic volc.	three classes established based on empirical class breaks (>5 km = low(1), 5-0.001 = medium(2), <0.001 km = high(3))	0.99	0.68	0.68	0.458
				distance to EOd31 - undiff. mafic-felsic volc.	three classes established based on empirical class breaks (>5 km = low(1), 5-0.001 = medium(2), <0.001 km = high(3))	0.99	0.68	0.5	0.337
				distance to EOd9 - intermediate felsic intrusions, Eodc - marcollat granite, Enm - Marne River Volc., Eody - Murray Bridge Granite, ED - undiff. maf-int intrusions, EOd19 - undiff. dioritic intr, Eod - undiff. mafic-felsic intrusives, EOd25 -undiff. granitic-granodioritic intrusions, Eod4 - undiff. felsic volc., Eod1 - undiff. felsic volc.	three classes established based on empirical class breaks (>5 km = low(1), 5-0.001 = medium(2), <0.001 km = high(3))	0.99	0.68	0.3	0.202
				distance to Eodo - mount monster porphyry	three classes established based on empirical class breaks (>5 km = low(1), 5-0.001 = medium(2), <0.001 km = high(3))	0.99	0.68	0.11	0.074
			largely intermediate to felsic volcanics and intrusives possibly related to subduction or post-subduction extension	distance to Eod4 - def meta granite tonalite, Eod - mafic-felsic intrusions, Eod1 - undiff. mafic-felsic volc., Eod31 - undiff. interm.-mafic volc.	three classes established based on empirical class breaks (>5 km = low(1), 5-0.001 = medium(2), <0.001 km = high(3))	0.99	0.5	0.3	0.149
				distance to Eode - Encounter Bay Granite, Ek4 -undiff. mafic-felsic volc.	three classes established based on empirical class breaks (>5 km = low(1), 5-0.001 = medium(2), <0.001 km = high(3))	0.99	0.5	0.11	0.054

Mineral system component	Process	Critical component theoretical	Critical component mappable	Derivation of mappable critical components	Classes within the evidential layer	Importance weight	Applicability weight	Confidence weight	Overall weight
			mafic and intermediate volcanics, felsic intrusions not related to subduction or post subduction extension, mixed volcanosedimentary units	distance to Egn - Gnalta Group (minor interm. volc.), NE3 - undiff. mafic-felsic volc. and seds.	three classes established based on empirical class breaks (>5 km = low(1), 5-0.001 = medium(2), <0.001 km = high(3))	0.99	0.3	0.3	0.089
				distance to N-wbox - Boucaut Volc., Eodt - Taratap Granodiorite, Eod26 - mafic-ultramaf. intr., Eo9 - undiff. mafic volc., Ek3 - dolerite, basalt, Eod4 – undiff. mafic-felsic volc., Ek4 - undiff. mafic-felsic volc. and metas, Eo9 - undiff. mafic-felsic volc.	three classes established based on empirical class breaks (>5 km = low(1), 5-0.001 = medium(2), <0.001 km = high(3))	0.99	0.3	0.11	0.033
			mafic volcanic suites associated with possible arc or post-subduction extension	distance to Eod23 - metagabbro-dolerite, NE3 - undiff. mafic volc., seds	three classes established based on empirical class breaks (>5 km = low(1), 5-0.001 = medium(2), <0.001 km = high(3))	0.99	0.11	0.11	0.012
		hydrous mafic magmatic bodies and fertile SCLM as source regions for metals, sulphur, chlorine and water	low resistivity zones at 50 km depth	classified raster of MT resistivity at 50 km depth projected to the surface	z-score log transformed six classes established based on standard deviation from the mean (<-2.5sd (low), -2.5 to -1.5, -1.5- to -0.5, -0.5 - 0.5, 0.5 - 1.5, >1.5 (high))	0.99	0.83	0.5	0.411
		hydrous intermediate-felsic magmatic bodies in the middle crust, representing melt ponding	low resistivity zones in the middle crust	classified raster of MT minimum resistivity between 15-20 km depth projected to the surface	z-score log transformed seven classes established based on standard deviation from the mean (<-2.5sd (low), -2.5 to -1.5, -1.5- to -0.5, -0.5 - 0.5, 0.5 - 1.5, 1.5-2.5, >2.5 (high))	0.99	0.83	0.5	0.411
Crustal architecture	Deep structural features that affect magma ascent through crust, intermittent barriers, and conduits	deep seated, often cryptic, mostly transverse faults, misoriented, oblique structures can act as intermittent barriers for magma ponding and fluid flow	deep, gravity derived, orogen oblique structures	distance to orogen oblique crustal-scale structures	six classes based on empirical class breaks (>7.5 km (low), 7.5-6, 6-4.5, 4.5-3, 3-1.5, < 1.5 km (high))	0.68	0.68	0.5	0.231
			deep, gravity derived, orogen parallel structures	distance to orogen parallel crustal scale structures	six classes based on empirical class breaks (>7.5 km (low), 7.5-6, 6-4.5, 4.5-3, 3-1.5, < 1.5 km (high))	0.68	0.5	0.5	0.170
			intersections of deep gravity derived structures	distance to intersections of crustal scale structures	six classes based on empirical class breaks (>7.5 km (low), 7.5-6, 6-4.5, 4.5-3, 3-1.5, < 1.5 km (high))	0.68	0.68	0.5	0.231
Depositional site	Metal precipitation from magmatic fluid release facilitated by gradients in pressure, temperature, pH, and availability of sulphur	mostly calc-alkaline or high-K calc-alkaline to alkaline intrusives and volcanics; hydrous oxidised nature	all intrusive and volcanic units considered as indicators for common fertility	distance to volcanic and intrusive units considered fertile	three classes established based on empirical class breaks (>0.5 km = low(1), 0.5-0.001 km = medium(2), <0.001 km = high(3))	0.5	0.83	0.83	0.344
		mostly metasedimentary host	carbonate rich metasediments	distance to carbonate abundant sc. (siliciclastic) sediments (N-wck, Nms)	three classes established based on empirical class breaks (>0.5 km = low(1), 0.5-0.001 km = medium(2), <0.001 km = high(3))	0.5	0.83	0.83	0.344

Mineral system component	Process	Critical component theoretical	Critical component mappable	Derivation of mappable critical components	Classes within the evidential layer	Importance weight	Applicability weight	Confidence weight	Overall weight
		rocks, that can act as chemical buffers, provide porosity or are prone to fracturing	carbonate or iron rich metasediments and intrusive/volcanic rocks	distance to partially calcareous, Fe-ox. rich, heterogenous sc. sediments (N-huye, N-wb, N-wc, E-on-h, N-wbds, N-hunt, N-hui, N-huyw)	three classes established based on empirical class breaks (>0.5 km = low(1), 0.5-0.001 km = medium(2), <0.001 km = high(3))	0.5	0.68	0.83	0.282
				distance to calc-silicate and ultramafic rocks (E-ok)	three classes established based on empirical class breaks (>0.5 km = low(1), 0.5-0.001 km = medium(2), <0.001 km = high(3))	0.5	0.68	0.68	0.231
			carbonate or organic material containing metasediments	distance to sc. sediments with minor calcareous, carbonaceous layers (N-huek, N-huep, N-hwsu, N-huik)	three classes established based on empirical class breaks (>0.5 km = low(1), 0.5-0.001 km = medium(2), <0.001 km = high(3))	0.5	0.5	0.83	0.208
				(N-wbo, NPgrk, E-ok - volcanics and sediments)				0.68	0.170
			siliciclastic metasediments	distance to sc. sediments (N-hueu, E-ok - sedimens and volcanics, N-huyp, E-oklt, N-huyw - diamictite, N-hue, NE1, NE2, E-o1, Ete, Epo)	three classes established based on empirical class breaks (>0.5 km = low(1), 0.5-0.001 km = medium(2), <0.001 km = high(3))	0.5	0.3	0.83	0.125
								0.68	0.102
								0.5	0.075
		localisation of possible buffering and sulphidation processes	lithological boundaries representing geochemical gradients	geochemical contrast	z-score log transformed seven classes established based on standard deviation from the mean (<-2.5sd (low), -2.5 to -1.5, -1.5- to -0.5, -0.5 - 0.5, 0.5 - 1.5, 1.5-2.5, >2.5 (high))	0.5	0.83	0.5	0.208
		localisation of fracturing processes	lithological boundaries representing rheological gradients	rheological contrast	z-score log transformed seven classes established based on standard deviation from the mean (<-2.5sd (low), -2.5 to -1.5, -1.5- to -0.5, -0.5 - 0.5, 0.5 - 1.5, 1.5-2.5, >2.5 (high))	0.5	0.68	0.5	0.170
		localisation of damage zones, fracturing and possible localised extension	changes in upper and middle crustal fault orientations	distance to fault bends >10deg	six classes based on empirical class breaks (>2.5 km (low), 2.5-2, 2-1.5, 1.5-1, 1-0.5, < 0.5 km (high))	0.5	0.5	0.68	0.170
				distance to fault bends 5-10 deg	six classes based on empirical class breaks (>1.25 km (low), 1.25-1, 1-0.75, 0.75-0.5, 0.5-0.25, <0.25km (high))	0.5	0.3	0.68	0.102
			magnetics derived first order faults that can reach deeper levels	distance faults middle crust	six classes based on empirical class breaks (>2.5 km (low), 2.5-2, 2-1.5, 1.5-1, 1-0.5, < 0.5 km (high))	0.5	0.83	0.68	0.282
			magnetics derived second order faults that are mostly upper crustal	distance faults upper crust	six classes based on empirical class breaks (>1.25 km (low), 1.25-1, 1-0.75, 0.75-0.5, 0.5-0.25, <0.25km (high))	0.5	0.68	0.68	0.231
			intersections of magnetics derived faults	distance fault intersections	six classes based on empirical class breaks (>2.5 km (low), 2.5-2, 2-1.5, 1.5-1, 1-0.5, < 0.5 km (high))	0.5	0.83	0.68	0.282

Critical components characterising the processes that affected the deposition of metals were derived from the geological interpretation of magnetic and gravity data, the new basement map of the area (Wise, 2020). For the lithostratigraphic units, distances were again calculated to several selection sets. Three classes were considered, the presence of the unit (highest prospectivity), a 500 m buffer zone (medium prospectivity) representing uncertainty in the location of the geological boundary and areas further than 500 m away (low prospectivity). The lithostratigraphic unit sets reflect a qualitative partitioning according to the content of reactive constituents such as carbonate sequences and relatively iron-rich units. Predominantly carbonate-containing metasediments and Fe-rich rock units were weighted highest while pure siliciclastic sediments received the lowest weighting. The confidence weighting was approximated using three weight categories obtained from a depth to basement map (Gouthas, 2020). Median depth for each lithostratigraphic unit was calculated. Units that are outcropping or their median depth is up to 100 m received the highest weighting. Consequently, units with median depth between 100 and 400 m were weighted as less confident, and units with a median depth of more than 400 m were assigned the lowest weight.
Often the contact zones of units with vastly different geochemical or rheological properties focus mineral precipitation, and so an attempt was made to assign relative geochemical reactivity and rheological competency to each lithology, following the process described by Occhipinti et al. (2020). Geochemical and rheological contrast layers were derived based on the absolute difference of reactivity or competency across each geological boundary. The absolute difference was used as the weighting parameter in a kernel density function passed over the geological contacts. Log transformation and standardisation was applied to the density layers before classification into six and seven classes, based on the standard deviation from the mean (+-0.5 SD, +-1.5 SD, +-2.5 SD). The lowest value class (-2.5 SD) was considered least prospective, while the highest (+2.5 SD) was most prospective.
Structural features that may localise hydrothermal fluid flow above and laterally away from the volcano-intrusive centres were extracted from the geological interpretation layers. These upper crustal features could be considered more brittle, creating localised brittle damage and extensional zones that provide space for mineral precipitation. Changes in fault geometry were assessed for the interpreted faults. Two layers were extracted for fault bends larger than 5 and 10 degrees, respectively. The higher angle bends with a larger zone of influence (up to 2500 m) were weighted as more applicable when compared to the lower angle ones (zone of influence = 1250 m). The reason for creating two categories was to set apart low angle bends that would probably result in less extensive dilation from higher angle structures where the generation of space and damage zones could be more significant. Six distance classes were calculated to the bends, with the proximal having the highest prospectivity value. Distances to the upper and middle crustal faults as well as their intersections, were also computed and utilised. Here again, six classes were created based on distance, with the proximal class considered most prospective. The zone of influence for the intersections and mid-crustal (larger) faults was set to 2500 m while it was 1250 m for upper-crustal faults.

3.2 The fuzzy inference network

The created critical component evidence layers can be combined in many ways, ranging from simple weighted overlay to linear or non-linear combinations based on parametric or non-parametric statistical methods when training data is available. In this case study, the fuzzy inference logic approach similar to that of Occhipinti et al. (2016; 2020) was used. First, each classified layer was converted into a fuzzy membership layer where values range between zero and one. Different membership functions can be used, including linear, sigmoidal, gaussian or polynomial, to reflect the process/evidence being evaluated. A linear membership function was applied since some of the non-

linear transformations to the raw values were conducted during reclassification. After the fuzzy membership step, weighting based on the applicability and confidence was applied. The whole network was implemented in ArcGIS ModelBuilder using readily available geoprocessing functions. The model parameters, including all the weights and fuzzy operators, are exposed and easily modifiable. Users can change these weighting parameters to create modified models that would upgrade or downgrade critical components or change how these are combined according to the conceptual model.
The fuzzy inference network structure follows the concept of the mineral systems analysis and groups processes/critical elements into conceptual branches. It combines the fertility/geodynamic throttle components, crustal architecture, and depositional site first in their network branches with fuzzy operators before a final overall combination (Fig. 4).

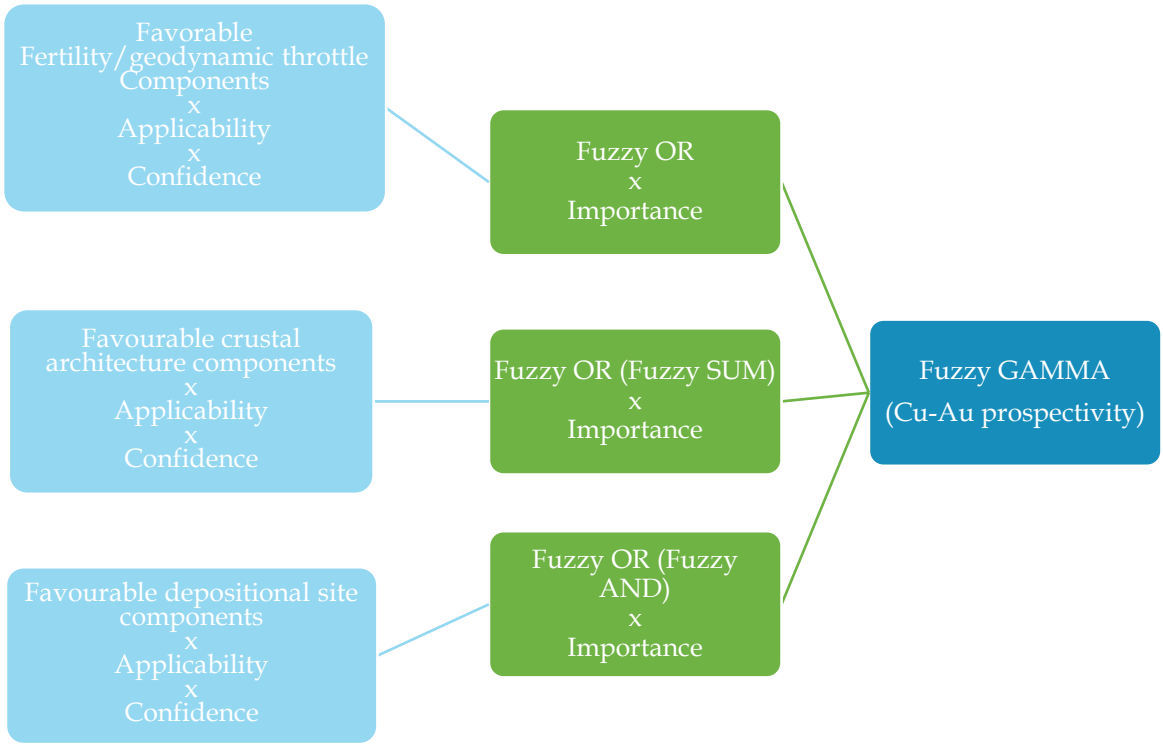

Figure 7 Schema of the fuzzy inference network components.

An importance weighting is used for the network branches. Fuzzy OR, AND, SUM, and GAMMA operators were used in the model. In the fertility/geodynamic throttle branch and map (Fig 5a), all the evaluations based on lithostratigraphy were first combined with an OR operator, which attributes the maximum value per cell. The source regions and ponding regions derived from the AusLAMP MT data (Robertson et al., 2020) were combined separately with another OR operator before a SUM operator combination with the lithostratigraphy fuzzy membership values. The SUM operator effectively adds the values together, but its formulation is defined so that it can never surpass the maximum value of one. The overall fertility/geodynamic throttle branch importance was determined to be the highest compared to the crustal architecture and depositional site branches. The crustal architecture branch and map (Fig. 5b) combines the oblique and parallel structures with an OR operator first and then enhances the prospectivity at fault intersections by using the SUM operator to add the intersections evidence layer. The crustal architecture branch was weighted with a medium importance weight.

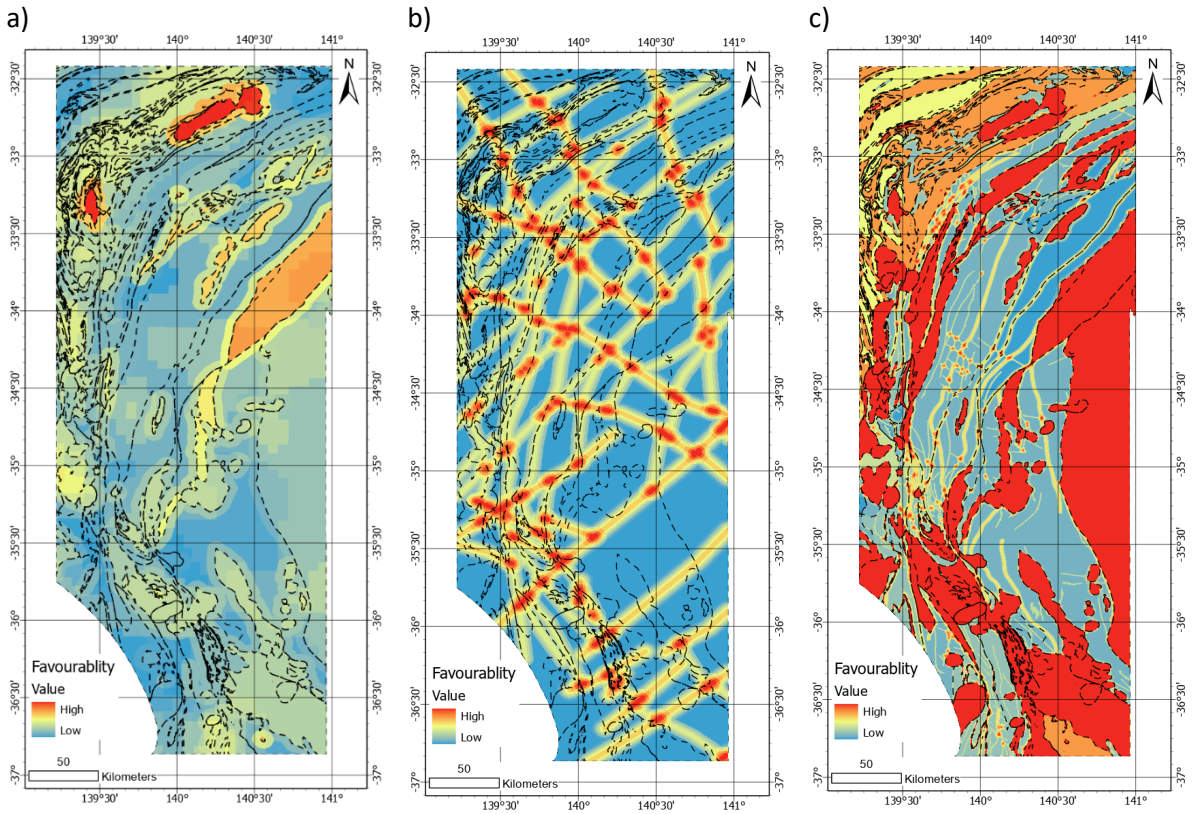

Figure 8 Intermediate favourability maps for a) fertility/geodynamic throttle, mainly highlighting the Anabama and Bendigo intrusions, but also the Mount Wright Volcanics and similarly old intrusive/volcanogenic rocks as well as AusLAMP MT conductors b) crustal-scale architecture highlighting intersections of structures and more and less prospective orogen oblique and orogen parallel discontinuities and c) depositional site, favouring felsic to intermediate intrusives, volcanics and reactive sedimentary units as well local structural features.

The lowest importance weight was attributed to the depositional site branch and map (Fig 5c). This branch first combined lithostratigraphic evidence layers and the geochemical contrast layer using an OR operator. The structural part of the branch was separately integrated using another OR function. Internally the structural features include an intermediate step where fault intersections were added to the mid and upper crustal faults utilising the SUM operator similarly to the processes in the crustal architecture component. The structural and geochemical evidence layers were combined with an OR operator, but an AND operator was also assessed. This alternative model tests the option that high favourability values in both the structural and geochemical depositional gradients are needed to mark an overall favourable depositional site.
In the final step, all branches were combined using a fuzzy GAMMA function. Setting the GAMMA value is best suited for adjusting for integrating evidence layers stemming from different modalities with different associated confidence measures. The gamma parameter was left at its default value of 0.9.

4 Results & Discussion

The newly created prospectivity maps highlight several regions that could be considered for follow-up work to confirm the conceptual mineral system model. The classification scale used on the resulting maps copies the classification of the Sherman-Kent scale (Tab. 1), omitting the top and bottom classes and incorporating them into the neighbouring class. The six classes represent 0-20, 20-40, 40-60, 60-75, 75-90, 90-100 percent of the prospectivity values, respectively.

The final best prospectivity map (Fig. 9a) identifies parts of the most fertile lithostratigraphic units that coincide with major crustal-scale structures and possible gradients in rock competency and geochemical composition. Existing copper and gold occurrences (of various deposit styles) mostly fall within, or close to, zones that are mapped as likely or very likely prospective (Figure 9a), indicating that a degree of commonality may exist in the causative structures and formations for multiple deposit styles.

The most prospective regions highlight parts of the Anabama Hill intrusion and the Bendigo intrusion as well as the interpreted extent of the Mount Wright Volcanics. Several smaller possible prospective zones can also be found in the other undifferentiated granitoid intrusions and the interpreted Bittles Tank Volcanics. The prospective zones in the Murray Bridge Granite, which is most probably post-orogenic A-type intrusion (Foden et al., 1996; Foden et al., 2020), could still indicate a post deformation more alkalic type of intrusion with similarities to PCDs (Richards, 2009). As Foden et al. (2020) points out, some post-subduction granites show fractionated character and high Sr/Y values consistent with fertile PCD related magmas; however, they might also be far too fractionated. Alternatively, the applied applicability weighting could be downgraded for the post-orogenic granites to rule out this mineral system model.

It should be noted that there are very few observable fault/shear structures in the exposed parts of the Delamerian Orogen that formed part of this study, potentially due to a strongly partitioned deformation (Wise, 2020). Folding is predominant in the exposed part with only associate small-scale faults that are difficult to recognise in potential field data. The result could be enhanced by accurately mapping at least fold closures or fold axes that were shown to be associated with gold occurrences in the area. Such an amendment could extend into the covered terrains; however, the folding will be generally less apparent. Epithermal copper and gold mineral systems are generally smaller-scale deposits than PCD's, and their formation may be more dependent on the local structural features and the presence of reactive rocks. Using the AND operator in the depositional site maps only zones close to the upper and mid-crustal structures within the prospective rock domains, which might not be ideal for the more significant deposits within the PCD system but might better highlight favourable areas for smaller epithermal and replacement type of deposits.

The classification of the volcanic and intrusive suites used to assess fertility was based purely on published data and reflected mainly descriptive characteristics of the intrusive suites. In covered areas, units were only attributed to a particular lithostratigraphy based on similarities in the magnetic character, shape, and position within the belt. Any additional information confirming the nature of the intrusive and volcanic suites would significantly improve the prospectivity map as new categorisation of these critical fertility components could be established. This can involve studies that would provide new geochemical, mineralogical, or isotopic data that all showed potential in discriminating between fertile and non-fertile magma compositions (John et al., 2010; Lee and Tang, 2020).

The importance of major crustal boundaries, which has been suggested by some authors (John et al. 2010; Hageman et al. 2016, Piquer et al., 2021), will be challenging to test. However, modelling and numerical simulation techniques can help ascertain whether the suggested fault geometries can reach deep lithospheric levels given the local petrophysical parameters and paleostress analysis. New petrophysical and structural data that would characterise the critical lithostratigraphic units and the paleo stress field would be essential for such tests. Depending on the modelling result, some suggested faults may be downgraded in their importance or wholly discarded.

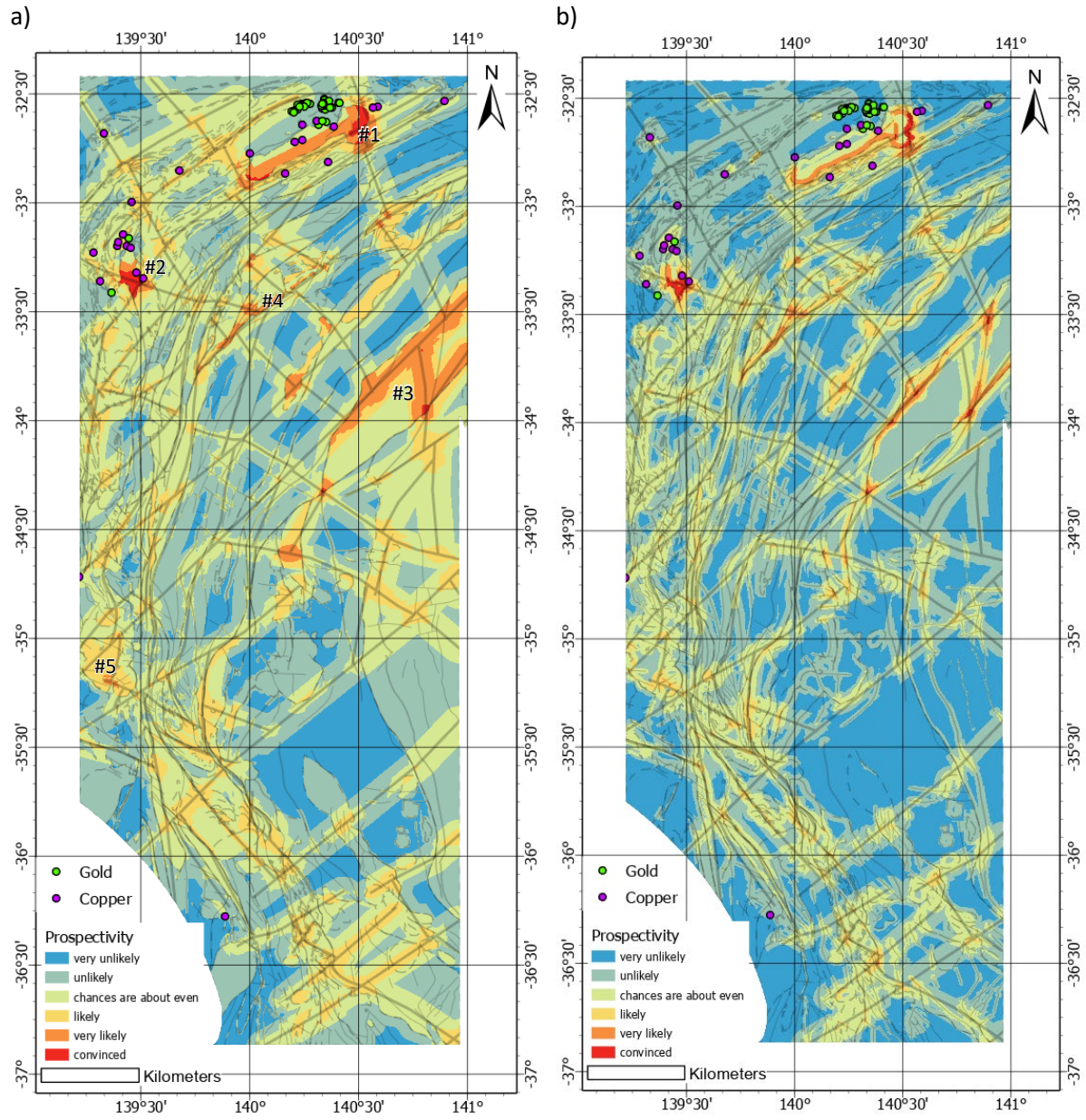

Figure 9a) Final prospectivity map for the Cu-Mo-Au mineral system b); an alternative model where depositional site structural and geochemical gradients were combined with a fuzzy AND operator. Locations: #1: Anabama Hill Intrusion, #2 - Bendigo Hill Intrusion, #3 Interpreted Mount Wright Volcanics, #4 Interpreted Bittles Tank Volcanics, #5 - Murray Bridge Granite Intrusion

5 Conclusions and recommendations

A mineral system analysis for Cu-Mo-Au in the Delamerian Orogen was conducted to assess its mineral potential. A conceptual model was delineated, and prospectivity maps were created. These maps can serve partially for drill and sampling campaign targeting. The conceptual model was implemented as a flexible workflow in ArcGIS that can be readily updated with new data.
Several critical elements of the conceptual model will be reassessed when more detailed geochemical, mineralogical, petrophysical, and structural data will be available after the MinEx NDI drilling?

The fractionation and oxidation state of the mapped intrusive/volcanic bodies will be better estimated by direct measurement and new sampling achieved during drilling and the associated surface mapping campaigns. Of primary interest should be the extent and nature of the interpreted Mount Wright Volcanics and other contemporaneous intrusive and volcanic suites related to the Delamerian arc or back-arc development.
These primary interest zones can be further narrowed down to spaces close to the interpreted major crustal discontinuities. Numerical simulation and 3D geological modelling will confirm or disprove the proposed model, which supports structures traversing most of the lithospheric crust.

6 Acknowledgements

The work has been supported by the Mineral Exploration Cooperative Research Centre, whose activities are funded by the Australian Government's Cooperative Research Centre Program. This is MinExCRC Document 20**/***

7 References

Alias, G., Sandiford, M., Hand, M., Worley, B., 2002. The P-T record of synchronous magmatism, metamorphism and deformation at Petrel Cove, southern Adelaide Fold Belt. Journal of Metamorphic Geology 20, 351–363.

Baatar, B., Parra-Avila, L.A., Fiorentini, M.L., Polito, P., Crawford, A.J., 2019. Porphyry Cu fertility of the Loch Lily-Kars Belt, western New South Wales, Australia. Australian Journal of Earth Sciences 67(1), 75–87.

Bookstrom, A.A., Glen, R.A., Hammarstrom, J.M., Robinson, G.R., Jr., Zientek, M.L., Drenth, B.J., Jaireth, S., Cossette, P.M., and Wallis, J.C., 2014. Porphyry copper assessment of eastern Australia: U.S. Geological Survey Scientific Investigations Report 2010–5090–L, 160 p. and GIS data, http://dx.doi.org/10.3133/sir20105090L.

Chiaradia, M., 2014. Copper enrichment in arc magmas controlled by overriding plate thickness. Nature Geosciences 7, 43–46.

Flöttmann, T., James, P., Rogers, J., Johnson, T., 1994. Early Palaeozoic foreland thrusting and basin reactivation at the Palaeo-Pacific margin of the southeastern Australian Precambrian craton: a reappraisal of the structural evolution of the Southern Adelaide Fold-Thrust Belt. Tectonophysics 234, 95–116.

Foden, J.D., Elburg M.A., Turner, S.P., Clark, C., Blades, M.L., Cox, G., Collins, A.S., Wolff, K., George, C., 2020. Cambro-Ordovician magmatism in the Delamerian Orogeny: Implications for tectonic development of the southern Gondwana margin. Gondwana Research, 81, pp.490–521

Foden, J.D., Elburg, M.A., Turner, S.P., Sandiford, M., O'Callaghan, J., Mitchell, S., 2002. Granite production in the Delamerian Orogen, South Australia. Journal of the Geological Society, London, 159: 557-575.

Gouthas, G., 2020. Delamerian Cover Thickness Modelling. Department for Energy and Mining. Geoscience Data Package, 00113.

John, D.A., Ayuso, R.A., Barton, M.D., Blakely, R.J., Bodnar, R.J., Dilles, J.H., Gray, Floyd, Graybeal, F.T., Mars, J.C., McPhee, D.K., Seal, R.R., Taylor, R.D., Vikre, P.G., 2010. Porphyry copper deposit model, chap. B of Mineral deposit models for resource assessment: U.S. Geological Survey Scientific Investigations Report 2010–5070–B, 169 p.

Jones, R.M., Hillis, R.R., 2003. An integrated, quantitative approach to assessing fault-seal risk. AAPG Bulletin 87 (3), 507–524.

Katona, L.F. 2020. Delamerian gravity and TMI datasets. Department for Energy and Mining. Geoscience Data Package, 00115.
Lee, C.-T.A., Tang, M., 2020. How to make porphyry copper deposits. Earth Planet. Sci. Lett. 529, 115868.
Mccuaig, T.C., Beresford, S., Hronsky, J., 2010. Translating the mineral systems approach into an effective exploration targeting system. Ore Geology Reviews 38, 128–138.
Occhipinti, S., Metelka, V., Lindsay, M., Aitken, A., Pirajno, F., Tyler, I., 2020. The evolution from plate margin to intraplate mineral systems in the Capricorn Orogen, links to prospectivity. Ore Geology Reviews 127, 103811.
Occhipinti, S.A., Metelka, V., Lindsay, M.D., Hollis, J.A., Aitken, A.R.A., Tyler, I.M., Miller, J.M., McCuaig, T.C., 2016. Multicommodity mineral systems analysis highlighting mineral prospectivity in the Halls Creek Orogen. Ore Geology Reviews 72(1), 86–113.
Piquer, J., Sanchez-Alfaro, P., Pérez-Flores, P., 2021. A new model for the optimal structural context for giant porphyry copper deposit formation. Geology 49, 597–601.
Raymond, O.L., Totterdell, J.M., Stewart, A.J., Woods, M.A., 2018. Australian geological provinces, dataset. 2018.01 edn. Geoscience Australia, Canberra.
Richards, J.P., 2009. Post-subduction porphyry Cu-Au and epithermal Au deposits—Products of remelting of subduction modified lithosphere. Geology 37, 247–250.
Richards, J.P., 2013. Giant ore deposits formed by optimal alignments and combinations of geological processes. Nature Geoscience 6, 911–916.
Robertson, K.E., Kirkby, A., Thiel, S., Duan, J. 2020. Delamerian AusLAMP Model. Department for Energy and Mining. Geoscience Data Package, 00112
Rosenbaum, G., 2018. The Tasmanides: Phanerozoic tectonic evolution of eastern Australia. Annual Review Earth and Planetary Science Letters 46, 291–325.
Selway, K., 2014. On the Causes of Electrical Conductivity Anomalies in Tectonically Stable Lithosphere. Surveys in Geophysics 35, 219–257.
Sillitoe, R.H., 2010. Porphyry copper systems. Economic Geology 105, 3–41.
Wilkinson, J.J., 2013. Triggers for the formation of porphyry ore deposits in magmatic arcs. Nature Geosciences 6, 917-925.
Wise, T. 2020. Interpreted basement geology to the Murray Basin and surrounds. Government of South Australia. Department for Energy and Mining DIGIMAP 00098.